Research article

A convolutional neural network model detecting lasting behavioral changes in mice with kanamycin-induced unilateral inner ear dysfunction

Masao Noda [a,b,1,*], Ryota Koshu [b], Dias Mari Shimada [b], Chortip Sajjaviriya [a], Chizu Saito [b], Makoto Ito [b], Taka-aki Koshimizu [a,**]

[a] Division of Molecular Pharmacology, Department of Pharmacology, Jichi Medical University, Japan
[b] Department of Otolaryngology and Head and Neck Surgery, Jichi Medical University, Japan

A R T I C L E   I N F O

A B S T R A C T

In acute aminoglycoside ototoxicity of the unilateral inner ear, physical abnormalities, such as nystagmus and postural alteration, are relieved within a few days by neural compensation. To examine exploratory behavior over an extended period, behaviors of freely moving mice after unilateral kanamycin injection into the inner ear were recorded in a home cage environment. The tail was excluded from deep learning-mediated object detection because of its delayed movement relative to the body. All detection results were confirmed using a convolutional neural network classification model. In kanamycin-injected mice, the total distance moved in 15 min increased on postoperative day 3. Furthermore, injured mice turned more frequently toward the healthy side up to 17 days after the surgery. This tendency resulted in increased clockwise movements in home cage recordings. Moreover, tail suspension and twisting toward the healthy side induced a physical sign for up to 14 days after the injury; the mice rapidly rotated with dorsal bending. Our analysis strategy employing deep learning helps to evaluate neuronal compensatory processes for an extended period and is useful for assessing the efficacy of therapeutic interventions.

1. Introduction

Ototoxicity of aminoglycoside antibiotics can cause serious side effects in vestibulocochlear organs, leading to balance and hearing dysfunctions [1,2]. A challenge of aminoglycoside-induced inner ear dysfunction is its unpredictability. In contrast to aminoglycoside-induced dose-dependent nephrotoxicity, no apparent association has been detected between the serum concentrations of the drug and the degree of vestibulotoxicity [3–5]. In clinical situations, close monitoring of patients treated with aminoglycosides is recommended for the early detection of the drug's side effects. Novel, effective monitoring approaches are actively explored [4], and new animal models and analysis methods are needed to better understand the ototoxicity of aminoglycosides.

The initial objective sign of an aminoglycoside-induced inner ear dysfunction can start on one side, and unilateral dysfunction is more difficult to detect than bilateral severe disease, especially in children and older adults [6–8]. Initial hearing loss occurs in the

* Corresponding author. Division of Molecular Pharmacology, Department of Pharmacology, Jichi Medical University, Tochigi, 329-0498, Japan.
** Corresponding author. Department of Pharmacology, Jichi Medical University, Tochigi, 329-0498, Japan.
E-mail addresses: doforanabdosuc@gmail.com (M. Noda), t_koshi@jichi.ac.jp (T.-a. Koshimizu).
[1] Lead contact: Masao Noda M.D., Ph.D., MBA E-mail: doforanabdosuc@gmail.com

high-frequency range because aminoglycosides damage hair cells in the cochlea's basal turn [9]. Acute hearing loss on one side results in a semipermanent failure of sound source localization and discrimination [10]. Persistent unilateral hearing loss may cause difficulty engaging in complex conversations in noisy environments for socialization, learning, and productive working [11]. Clinically, unilateral hearing loss may be due to several conditions, such as sudden injury, Meniere's disease, or early stage of bilateral hearing loss. Surgical or medical treatment may be used in its management; however, if there is no improvement, hearing aids or cochlear implants are some of the few effective options [12–16].

Aminoglycoside-induced hearing loss is a lasting disability; however, previous studies in rodents revealed that behavioral phenotypes and signs such as nystagmus due to acute unilateral balance dysfunction last approximately 1 week after the injury [17,18]. Hearing and balance dysfunctions of peripheral origin are known to undergo a central compensation process because the central integration of inputs from both sides of the peripheral and central components controls these two functions [10,11,17,19]. However, vestibular compensation is poor in some patients, and a relationship between remaining vestibular function and hearing loss requires a better knowledge of the recovery process using proper animal models [20,21].

This study in mice unilaterally introduced aminoglycoside-induced injury to the inner ear, and the compensatory recovery process was examined using the open field test for >1 week postoperatively. A deep learning analysis was developed to localize the mice. In prior open field experiments, plain floors with high-contrast backgrounds were used without bedding [22–25]. One of the difficulties of object detection in animal experiments is the constantly changing background environment if the cage floor's bedding is included. In the present study, mice were detected in cages with normal bedding because the bedding amount and condition critically impact animal behavior [26–28]. Furthermore, our analysis examined lasting behavioral changes beyond 1 week postoperatively in mice with aminoglycoside-induced unilateral inner ear injury.

2. Materials and methods

2.1. Animals and surgical procedure

In total, 40 male C57BL/6J mice aged 9 weeks were obtained from CREA Japan Inc. (Tokyo, Japan). All mice were housed under a 12-h light/dark cycle with food and water ad libitum in cages with floors covered by wood shavings as bedding material. The temperature of the animal room was controlled at 23 $\pm$ 1 °C, and the humidity at 55 $\pm$ 10 %. The protocols of all animal studies were approved by the Committee on Animal Research at Jichi Medical University in Shimotsuke, Japan (approval no 24099-01). The experiments were conducted following the Public Health Service Policy on Humane Care and Use of Laboratory Animals. We confirm that the details of this study are reported following the ARRIVE guidelines (https://arriveguidelines.org).

The surgical procedure for generating the deafness model has been reported previously [29–31]. A mixture of 0.75 mg/kg medetomidine, 4 mg/kg midazolam, and 5 mg/kg butorphanol was injected into the intraperitoneal space to induce anesthesia. We always operated on the left ear, leaving the right ear untreated. After creating a retro auricular incision, the tympanic capsule was drilled, and the round window membrane was exposed. Subsequently, 1 μL of 30 % kanamycin solution (weight/volume, dissolved in saline) was gradually injected into the cochlea through the round window membrane using a micro syringe (701N; 26s needle, Hamilton Co., Reno, NV, USA). During the recovery from this operation, 7 mice were lost. We divided the experiment into two parts (Fig. 1). In the first series of the experiment, 9 and 7 mice of the control and kanamycin groups, respectively, were analyzed by an experimenter in the open field test. Unilateral inner ear dysfunction was confirmed using the auditory brainstem response (ABR) on day 14 postoperatively. Subsequently, the inner ear specimens were histologically analyzed. In the second series of the experiment, 9 and 8 mice of the control and kanamycin groups, respectively, were analyzed in the open field test using a convolutional neural network (CNN) model on days 3, 7, and 17 postoperatively.
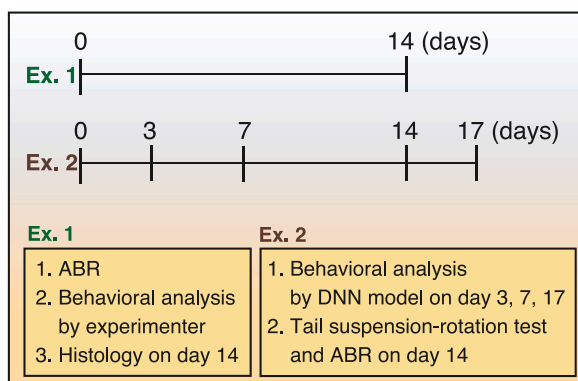

Fig. 1. Study outline. In the first series of experiments (Ex. 1), unilateral inner ear dysfunction was confirmed based on the auditory brainstem response (ABR) on day 14 postoperatively. After the ABR, the open field test by an experimenter, and a histological analysis were performed. In the second series of the experiments (Ex. 2), behaviors in the open field test were analyzed using the CNN model on days 3, 7, and 17 postoperatively. On day 14 in Ex. 2, the tail suspension-rotation test was recorded in a video, and the ABR was measured.

2.2. Auditory brainstem response measurement

The ABR was obtained in a sound-attenuated room 14 days after injecting kanamycin into the cochlea, as reported previously [32]. Subdermal needle electrodes were placed under anesthesia at the vertex and in the left and right mastoids. The threshold was evaluated based on the audiometry of the click-evoked ABR using the Tucker–Davis Technologies and Scope software (PowerLab; AD Instruments Japan, Aichi, Japan).

2.3. Histology

After the behavioral and ABR tests, the mice were perfused with 4 % paraformaldehyde in phosphate-buffered saline, and their inner ears were collected. The temporal bones were locally perfused and fixed in 4 % paraformaldehyde overnight at 4 °C, rinsed in phosphate-buffered saline, and dehydrated for 30 min at each step using once 30 %, 50 %, 70 %, 85 %, and 95 % ethanol and twice 100 % ethanol. The clearing was conducted twice, using xylol for 1 h. The specimens were subsequently immersed twice in liquid paraffin (1 h at 42–46 °C), embedded in a solid paraffin block, and incubated at 46–52 °C for 1 day. Deparaffinization was performed in a graded series for 5 min at each step using once 30 %, 50 %, 70 %, 85 %, and 95 % ethanol and twice 100 % ethanol. The specimens were subsequently rinsed twice with distilled water for 5 min and cut into 4-μm sections using the Microm HM340E microtome (Thermo Fisher Scientific, Waltham, MA, USA). The cross-sections were stained with hematoxylin and eosin. Histological analysis and image acquisition were conducted using the Olympus BX51 microscope (Olympus, Kyoto, Japan).

2.4. Open field test

We evaluated the locomotor and exploratory activities of mice in the open field test in a new polycarbonate cage (18 cm × 26 cm × 12 cm) with heat-treated wood shaving bedding. The behavior was recorded for 15 min using a video camera (Victor, model GZ-MG77S; JVC, Yokohama, Japan) at 30 fps and 640 × 480 pixels per image. The behavior on day 14 was evaluated based on human observation and on days 3, 7, and 17 using a deep learning model. For the human observation, the number of times of head tossing, sniffing, and touching the wall and the time spent in the center area were counted thrice for each mouse, and the average was used.
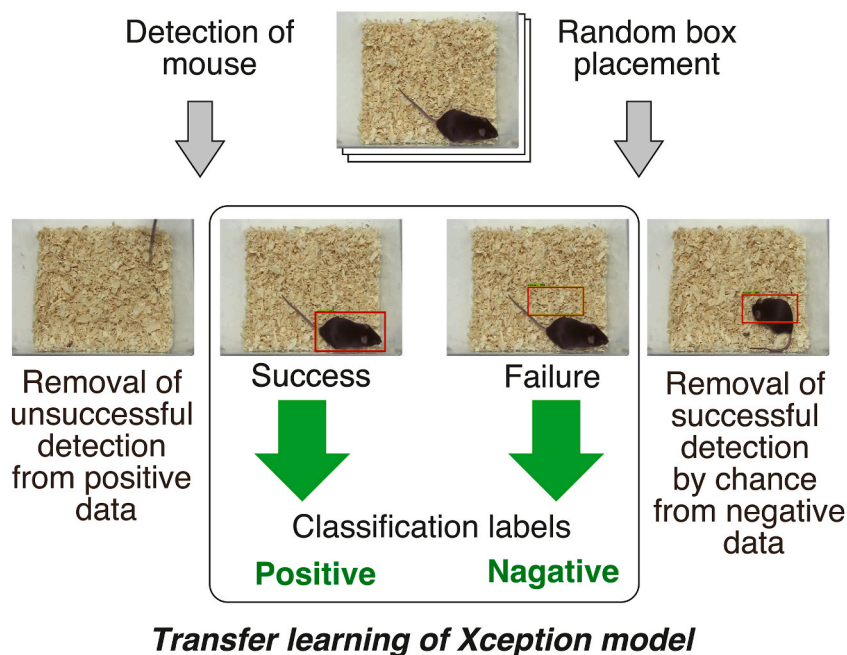

Fig. 2. Schematic flow of training deep learning model for the evaluation of object detection results. Custom dataset of images contained a mouse in the home cage with natural bedding. Mouse images with correct bounding box were generated our object detection program. Images of failed detection were manually removed from the "positive" training data. Images with negative detection were generated by placing a box in a random position. If by chance a box was placed on the mouse, such an image was manually removed from the "negative" group. Images with correct "positive" and "negative" labels were used for transfer learning of the *Xception* model, which was pretrained on Imagenet. The resultant model was used for image classification to evaluate the success/failure of mouse detection.

2.5. Detection of mouse movements

For the automated calculation of mouse movements, sequential images from video recordings were obtained at five images per second. The locations of mice in training images were identified and boxed using the LabelImg software (Tzutalin; https://github.com/tzutalin/labelImg). We used 5682 images with labels, randomly partitioned into training/validation (90 %) and test (10 %) sets. We used transfer learning using the single-shot multi-box detector ResNet50 (SSD_ResNet50), pretrained on the COCO 2017 dataset, available from the TensorFlow 2 Detection Model Zoo (https://github.com/tensorflow/models/blob/master/research/object_detection/g3doc/tf2_detection_zoo.md) [32,33]. The training and evaluation steps were performed in the TensorFlow version 2.2 environment and Object Detection API (Google, Inc., Mountain View, CA, USA) [34]. For the Python code, we referred to the website instructions at https://tensorflow-object-detection-api-tutorial.readthedocs.io/en/2.2.0/. The code was developed using a MacBook Pro with CPU support (Apple Inc. OS 12.7) and transferred to the Ubuntu 20.04 operating system with a Nvidia A6000 GPU, which was established in a Conda environment. The Conda environment file with a list of software packages has been uploaded to the Harvard Dataverse (see the Data Availability Statement section). After the transfer learning, our model achieved an 87 % mean average precision value. In addition, when hand-written bounding boxes for ground truth were prepared and compared to the tail-minus detection results in 1045 images, detected boxes are very close to the ground truth bounding boxes; calculated Intersection over Union value (IOU) was 79.5 ± 0.5 %. Notably, all detections were more than 50 % in IOU, indicating high and steady detection capacity of our model. The x-y coordinates of the center of the detected bounding box were considered the location of the mouse. Distances and angles of movements from each image to the next were calculated using Python and were plotted using the ggplot2 package in the R statistics environment (version 4.1.2; The R Foundation, Vienna, Austria) [35,36]. Movements in the open field test were expressed as relative distances, and the maximum width and height of the image were 1 in each set. This manipulation resized the output square during TensorFlow calculation, but actual size of the cage floor was 18 cm × 26 cm, as mentioned above.

2.6. Evaluating the detection accuracy using a deep learning classification model

The success or failure of detecting the mouse was evaluated using an independently developed deep learning classification model. The transfer learning was performed using the *Xception* model pretrained with Imagenet and fine-tuned using custom data of 8000 training, 1600 evaluation, and 1600 test images (Fig. 2). The mouse was detected with a bounding box, and these images were used with a successful "positive" label for model training. Images of detection failure were manually removed from the "positive" training material (Fig. 2). Images of failed detection with a "negative" label were generated by randomly placing a bounding box in an image. If by chance the bounding box contained a mouse, this image was removed from the "negative" training material (Fig. 2). The size of the bounding box in the failed images was fixed at 0.2 × 0.3 of relative height × width, where the maximum height and width of an image were set as 1. Therefore, an original mouse image usually produced "positive" and "negative" training materials with correct detection and random box placement, respectively. An example training code was obtained from the TensorFlow and Keras website (https://keras.io/examples/vision/retinanet/) [37]. Validation accuracy and loss values as well as detection scores were obtained from Tensorbord. The accuracy and loss values of the 1600 test images were 0.9994 and 0.0018, respectively. The receiver operating characteristic (ROC) curve was generated using separately labeled images of a sham mouse 14 days after surgery.

2.7. Tail suspension-rotation test

A mouse was suspended by pinching its tail, and then the tail was twisted clockwise to rotate the trunk of the mouse. After the rotation had stopped, the tail was twisted counterclockwise to return to the initial pinch position. The test was captured in a video, and recorded images were obtained one image per second. The angle between the tail and the longitudinal axis of the trunk was determined throughout the series of images in a test using a Python program (https://www.higashisalary.com/english/entry/python-calc-image-angle), and an image with the smallest angle was selected.

2.8. Data and statistical analyses

Data were expressed as the mean ± standard error of the mean. The R program was used for Student's t-test or Wilcoxon's test to compare the control and kanamycin groups. When the number of mice per group was less than or equal to five, the nonparametric Wilcoxon test was used. Time and drug (saline or kanamycin) were set as two factors, and the analysis of variance (ANOVA) was calculated to analyze the time course of open field tests. Statistical significance was set at $p < 0.05$.

3. Results

3.1. Functional and histological confirmation of kanamycin-induced unilateral inner ear injury

The deafness model was confirmed using ABR measurements 14 days after the kanamycin injection into the left cochlea. Click-evoked ABRs showed a profound lack of response in the left ear of kanamycin-injected mice, with the wave threshold reaching 80–90 dB (Fig. 3A). In contrast, the wave threshold of the saline group was approximately 30 dB (Fig. 3A). Furthermore, the ABR of the contralateral side in kanamycin-injected mice was within the normal range (Fig. 3A).

After the ABR recording, the experimenter analyzed the behaviors of the mice in video recordings of the open field test for 15 min
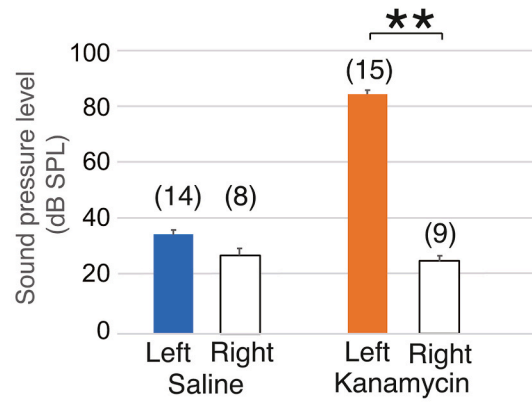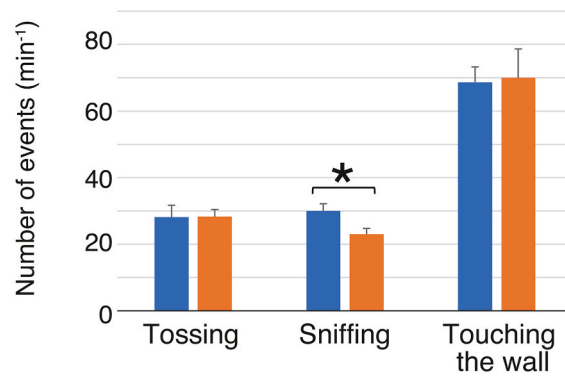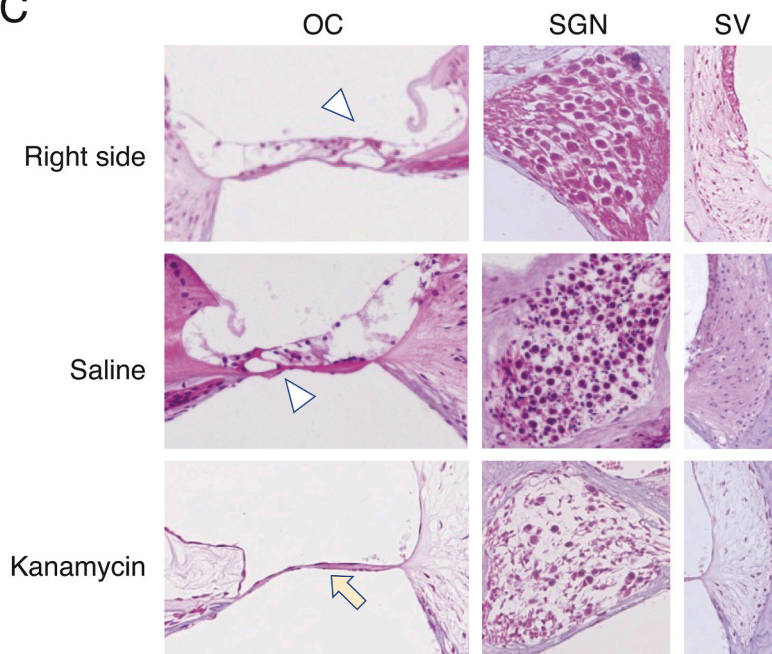
(caption on next page)

Fig. 3. Functional and histological confirmation of the unilateral left inner ear injury. (A) Saline or kanamycin was injected into the left inner ear, and the right side was not treated. The auditory brainstem response (ABR) was examined 14 days after the treatment. The ABRs in saline-treated control mice (left) show threshold waves at approximately 30 dB on both sides. In contrast, in the kanamycin-induced hearing-loss model (right), a large increase in sound pressure level was detected on the left side (orange). The numbers above the bars indicate the total numbers of ABR measurements from Ex. 1 and Ex. 2. In saline-injected mice, left and right sides were analyzed in 14 mice (9 and 5 mice in Ex. 1 and 2) and 8 mice (6 and 2 mice in Ex. 1 and 2), respectively. In kanamycin-injected mice, left and right sides were analyzed in 15 (8 and 7 in Ex. 1 and 2) and 9 (7 and 2 in Ex. 1 and 2) mice, respectively. *, $p < 0.05$; **, $p < 0.01$. (B) The sniffing behavior is reduced in mice with unilateral inner ear disorder 14 days after the injection. In the open field test, activities were counted for 15 min. The bar graphs show the activities in saline-control (blue, n = 9) and kanamycin injury (orange, n = 7) mice. *, $p < 0.05$. (C) Cochlear morphology was examined using hematoxylin and eosin staining on day 14 postoperatively, demonstrating the histopathology of the cochlear tissue in kanamycin-induced model mice. The images show cross-sections of the cochlea, organ of Corti (OC), spiral ganglion neurons (SGN), and stria vascularis (SV).

by gross counting. No significant difference was detected in head tossing (28.17 ± 3.53 and 28.20 ± 2.20 times, p = 0.99), touching the wall (68.7 ± 4.61 and 70.0 ± 8.64 times, p = 0.91), and counts of entry into the center area (35.6 ± 4.07 and 45.5 ± 8.65 times, p = 0.39) for the control and kanamycin-induced models, respectively. However, the count for sniffing in kanamycin-injected mice (23 ± 1.73 times) was significantly lower than that in saline-injected mice (30 ± 2.16 times; p = 0.025, t-test; Fig. 3B).

The cochlea structure on the right, noninjected side was intact in both saline- and kanamycin-injected mice (Fig. 3C). In fact, the organ of Corti, a tunnel formed by inner and outer hair cells, spiral ganglion, and stria vascularis were clearly recognized (Fig. 3C).
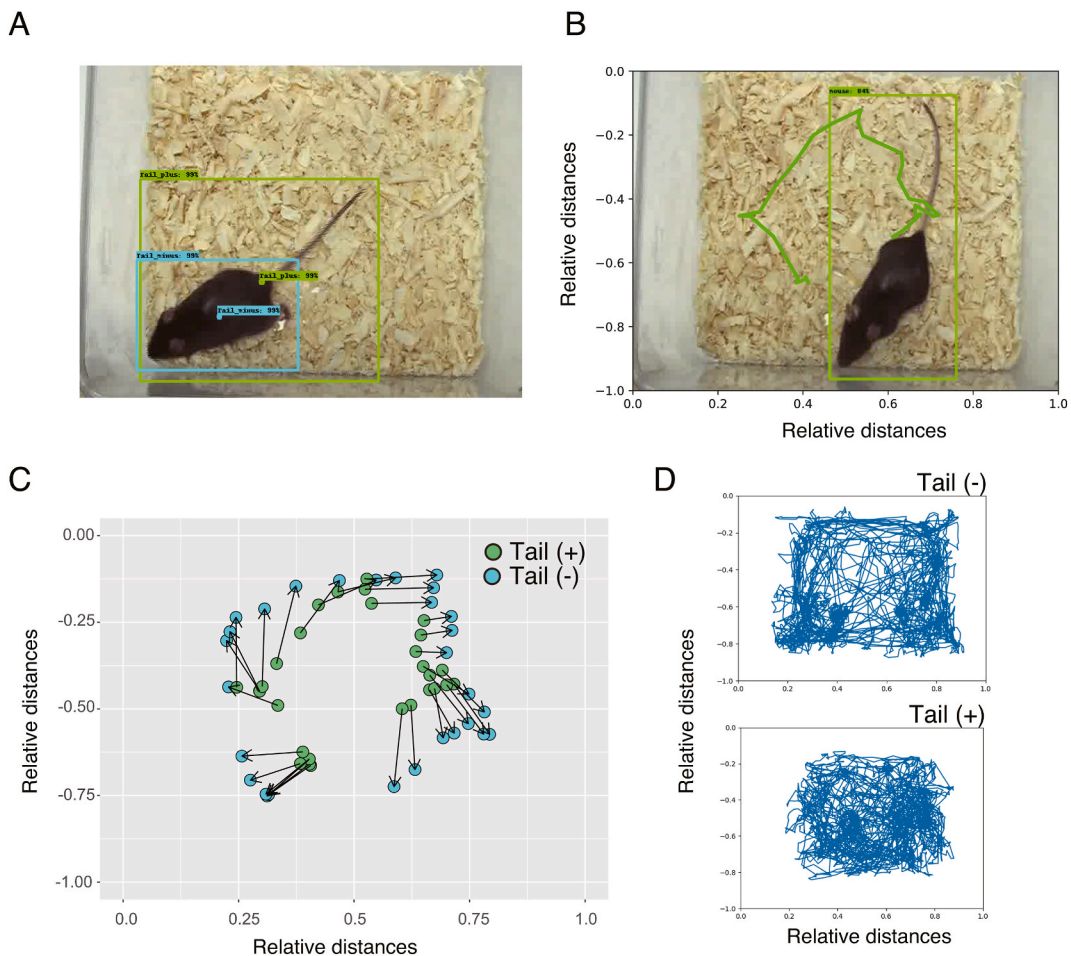

Fig. 4. Detection of mice excluding their tails improves movement tracing in the open field test. (A) Green and blue boxes indicate the detection of the mouse with and without its tail, respectively. Center points are indicated using the same colors. (B) A trace example of mouse movements. In this case, the mouse moved from the position shown in panel (A) to the one shown in (B) in a clockwise direction in 30 images. After plotting trace lines of the mouse movement in an image, X- and Y-axis ticks were included. (C) Differences between the center points with or without tail detection. A series of mouse images from the position in panel (A) to that in panel (B) were detected by the deep learning model, which include (green) or exclude (blue) the tail. The two types of center points in each image are connected by arrows. (D) The traces of mouse movements differ depending on the tail inclusion status. Using the same video recording of 15 min, the mouse was detected with or without the tail, and the movements of the center points were traced.

However, the cochlear morphology of the left ears of the kanamycin-induced injury model showed a collapse of the tunnel of hair cells and severe degeneration of the spiral ganglion (Fig. 3C).

3.2. For improved accuracy of movement traces, the mouse tail should be excluded from detection by the CNN

When analyzing detection results, we noticed that the inclusion of the mouse tail during object detection had a considerable effect on the location of the mouse center point and subsequent tracing because the tail pointed in various directions depending on the prior status of the mouse (Fig. 4A and B). We assumed that excluding the tail from a detection box might improve detection of the mouse movements. In fact, the centers with included tails were relatively posterior positioned and showed fewer movements compared to traces excluding the tail (Fig. 4C). The overall tracing patterns of control mice excluding their tails showed a clear preference close to the cage walls (thigmotaxis, Fig. 4D). Therefore, we employed a mouse detection method excluding the tail in all subsequent analyses.

3.3. Evaluating the object detection accuracy using the image classification model

Evaluating the accuracy of object detection is a difficult task because many images need to be examined. A possible method is to train a deep learning model, which can classify the success and failure of bounding box placement. Our classification model had high accuracy and low loss values during training (Fig. 5A and B). In the 4584 images from an open field test of 15 min, a part of the tripod used for the video recording was erroneously detected and boxed in 123 images (Fig. 5D). The classification model correctly classified the tripod detection as "negative". The ROC curve using the detection score as a threshold value showed a high area under the curve (AUC) of 0.98 (Fig. 5C). Among 232,742 images analyzed in this study, our classification model detected one negative image of actual failure (Fig. 5D). Such a failed image was excluded from the subsequent analysis. The lowest detection score was due to a mouse being partially covered by bedding material (Fig. 5E). Therefore, our object detection model showed high accuracy based on the deep learning-based classification.

3.4. The distance moved is increased on postoperative day 3 in the kanamycin-induced mouse model of unilateral inner ear dysfunction

Mice in the kanamycin group explored in the open field more distance than control mice 3 days after the surgery (Fig. 6). In further analyses, kanamycin injection and time course were identified as critical determinants of the distances moved (two-way ANOVA: $F(1,85) = 84.77$, $p < 0.0001$ for kanamycin/saline injection and $F(1,85) = 88.79$, $p < 0.0001$ for time course). No interaction was detected between treatment and time ($F(1,84) = 0.146$, $p = 0.703$). On day 7 postoperatively, the time course, but not kanamycin treatment, determined the distances moved (two-way ANOVA: $F(1,85) = 32.81$, $p < 0.0001$ for time course). In contrast, no statistical difference was detected in the distances moved on day 17 postoperatively.
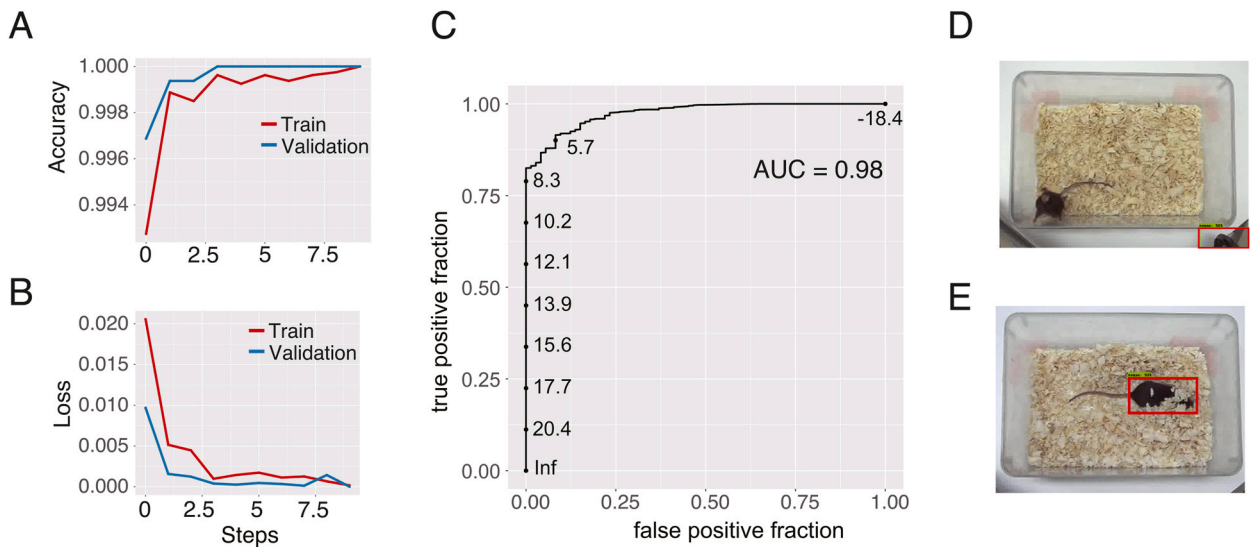

Fig. 5. Deep learning-mediated evaluation of object detection results. (A, B) Accuracy (A) and loss (B) values of the classification model. The model was trained to detect correct bounding box placement as described in the *Methods* section. A total of 8000 and 1600 images were used for training and validation, respectively. (C) The receiver operating characteristic (ROC) curve with threshold score was generated from a separate set of open field tests for 15 min each. AUC, area under the curve. (D) One image from unilateral inner ear injury mouse was classified as "negative," in which a tripod was detected as the mouse. This image was excluded from further analyses. (E) The lowest detection score was due to a mouse under the bedding. However, the detection was considered successful.
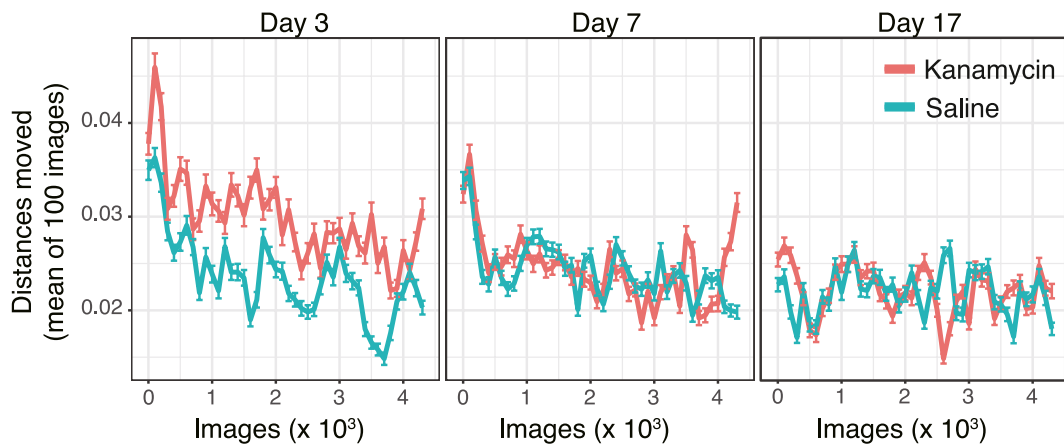
Fig. 6. Mice in the unilateral inner ear dysfunction group moved over longer distances in the open field test on day 3 postoperatively. The mouse behavior in the open field test was video-recorded for 15 min on days 3, 7, and 17 postoperatively, and the recording was converted to images at 5 images/s. The deep learning model localized the x-y coordinates of the mouse. The distances moved between two consecutive images were calculated, and the averaged distances from every 100 consecutive images were plotted against the sequential number of the images. Orange lines indicate the kanamycin-injected model (n = 8), and green lines indicate the control group (n = 9). Error bars show the standard error of the mean. The maximum width and height in an image were set as 1.

3.5. Kanamycin-injected mice turn to their healthy right side more frequently than to their injured left side

Based on the video recordings of freely moving mice in the open field test, we calculated the angles of their direction of movement (Fig. 7A and B) with three consecutive images defining an angle. The accumulated angles during the test were close to 0 in control mice, meaning the mouse turned to the right and left equally. However, mice with left inner ear dysfunction showed a clear tendency to turn more frequently to the right-hand side and move clockwise (Fig. 7C). Repeated open field tests revealed that the tendency of mice with left inner ear injury to turn clockwise was maintained even 17 days after surgery (Fig. 7C). In the open field test, treatment with kanamycin or saline was a significant determinant of the moving angle (two-way ANOVA: $F_{(1,84)} = 155.5$, $p < 0.001$; $F_{(1,84)} = 32.5$, $p < 0.05$; and $F_{(1,84)} = 26.74$, $p < 0.001$ for postoperative days 3, 7, and 17, respectively). Likewise, the time course of the open field test was a significant determinant (two-way ANOVA: $F_{(1,84)} = 13.5$, $p < 0.001$; $F_{(1,84)} = 426.9$, $p < 0.05$; and $F_{(1,84)} = 226.2$, $p < 0.001$ for postoperative days 3, 7, and 17, respectively). The two factors treatment and time course showed significant interactions on the moving angles ($F_{(1,84)} = 169.2$, $p < 0.001$; $F_{(1,84)} = 152.5$, $p < 0.001$; and $F_{(1,84)} = 191.6$, $p < 0.001$ for days 3, 7, and 17, respectively).

3.6. Kanamycin-injected mice move more frequently in a clockwise direction

The consequence of turning to the right more frequently in mice with left inner ear injury was further examined by visualizing and quantitating mouse movements in cages with natural bedding. We evaluated the direction of rotation during thigmotaxis which is the tendency of the mouse to move close to the walls. Lines for detecting mouse movement directions were set around the middle of each cage wall in four directions and close to the wall within a relative distance of 0.25. If a mouse crossed any of the four lines in the clockwise direction in the next image, the mouse position was colored green, and one point was added to the count (Fig. 8). Crossing in the opposite, counterclockwise direction resulted in purple points, and one point was subtracted from the counts. On day 7 postoperatively, unilateral injury mice showed a significant increase in the frequencies to turn in a clockwise direction, which was the side of the healthy ear (Fig. 8). The total counts of control and kanamycin mice were -0.7 ± 6.3 and 27.8 ± 10.5, respectively (t-test: t = -2.3232, df = 11.7, $p < 0.039$). The time spent in the center area in the open field is a measure of anxiety. However, the values for the time spent in the center area were similar in control and kanamycin-treated mice.

3.7. Tail suspension-rotation test for detecting unilateral inner ear injury

During the experiments, we noticed that when an injured mouse was transferred between cages by holding its tail, twisting the tail in a clockwise direction resulted in a fast rotation of the body with a strong dorsal bend (Supplementary Videos 1 and 2 showing control and injured mice, respectively). Measuring images from video recordings on day 14 postoperatively, we found that the angles between the tail and the longitudinal axis of the trunk were significantly smaller in kanamycin-injected mice than in the control mice (Wilcoxon's test: W = 30, $p < 0.01$; Fig. 9A and B). Suspending a mouse without rotation did not induce dorsal bending or fast rotation.
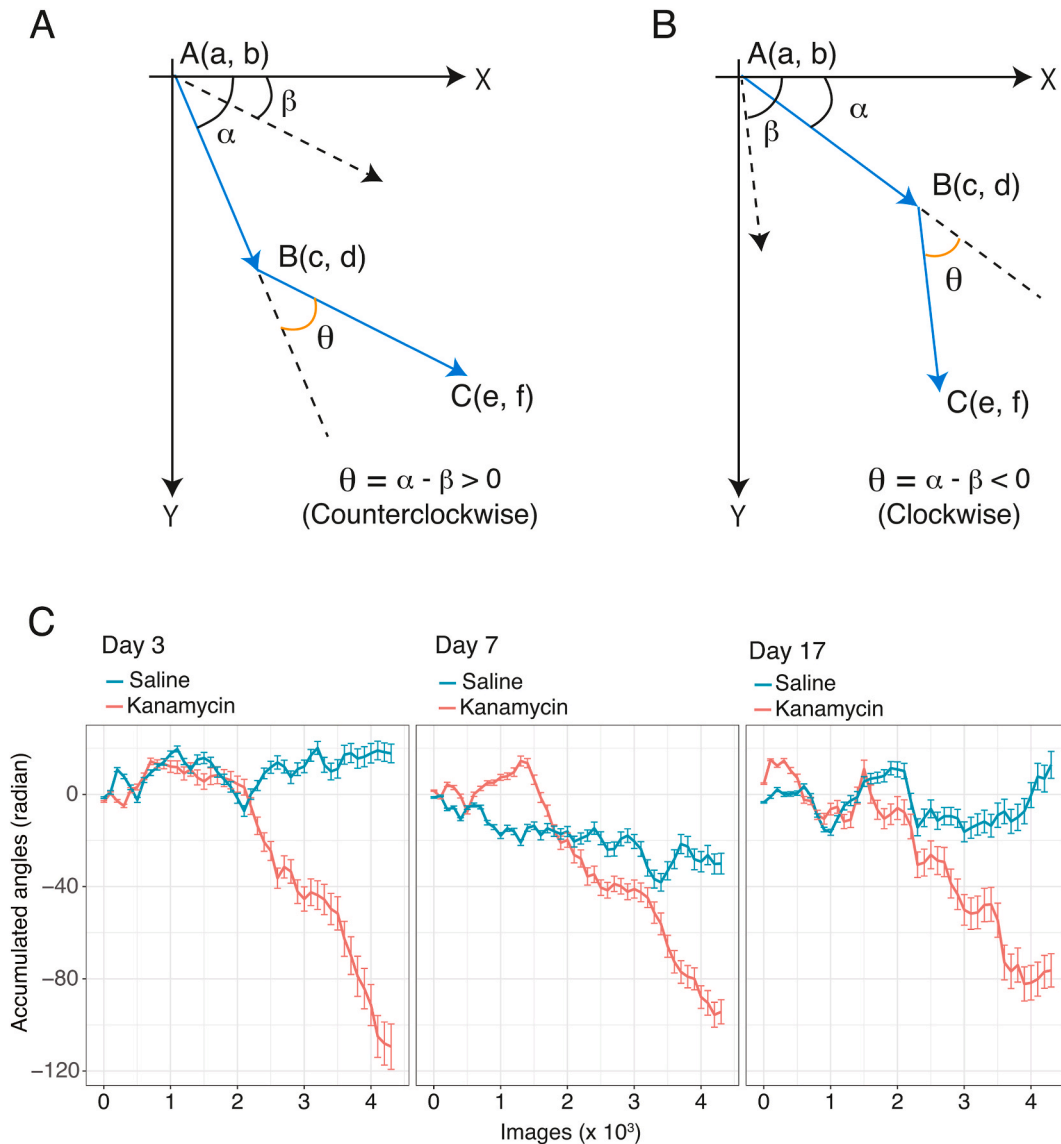
Fig. 7. Increase in clockwise rotation of mice with kanamycin-induced left inner ear injury. (A) and (B) show the calculation procedures of the moving direction in a mouse. The mouse proceeded from point A to B and then C in three consecutive images. The mouse position was localized as the center of the detection box in each image using the object detection of the deep learning model. Angle θ was calculated as angle α − angle β. The angle α is the angle between the x-axis and vector *AB*, and β is that between the x-axis and *BC*. From the x-y coordinates of the three points of the moving mouse, angles α and β were calculated using the atan2 function of the R program. Panels A and B show examples of counterclockwise (an increase in the angle θ, A) and clockwise (a decrease in the angle θ, B) directions. The origin of the x-y coordinates in TensorFlow was the left upper corner of an image. (C) Accumulated angles during the open field test are shown in mice with left inner ear injury (orange, n = 8) and in control mice (green, n = 9). The data are the mean ± standard deviation.

4. Discussion

This study assessed the behavioral abnormalities lasting >1 week in mice with unilateral inner ear disorders after kanamycin injection. Unilateral inner ear dysfunction, confirmed by ABR and histology, was correlated with a positive sign of the tail suspension-rotation test. Our efficient CNN model detected the mouse as an object and automated the analysis of open field behavior. For training the model, the mouse tail was excluded from the detection box to obtain the body's center point. This exclusion eliminated the influence of tail movement, which was delayed relative to the body's movement. The accuracy of the object detection was confirmed using an image classification CNN model for correctly placing the bounding box. Our analysis of the open field test revealed that kanamycin treatment increased the travel distance on day 3 postoperatively. A more lasting change was the movement tendency in the kanamycin group; the mice turned more frequently to the right, healthy side than the opposite, injured side. Furthermore, based on the
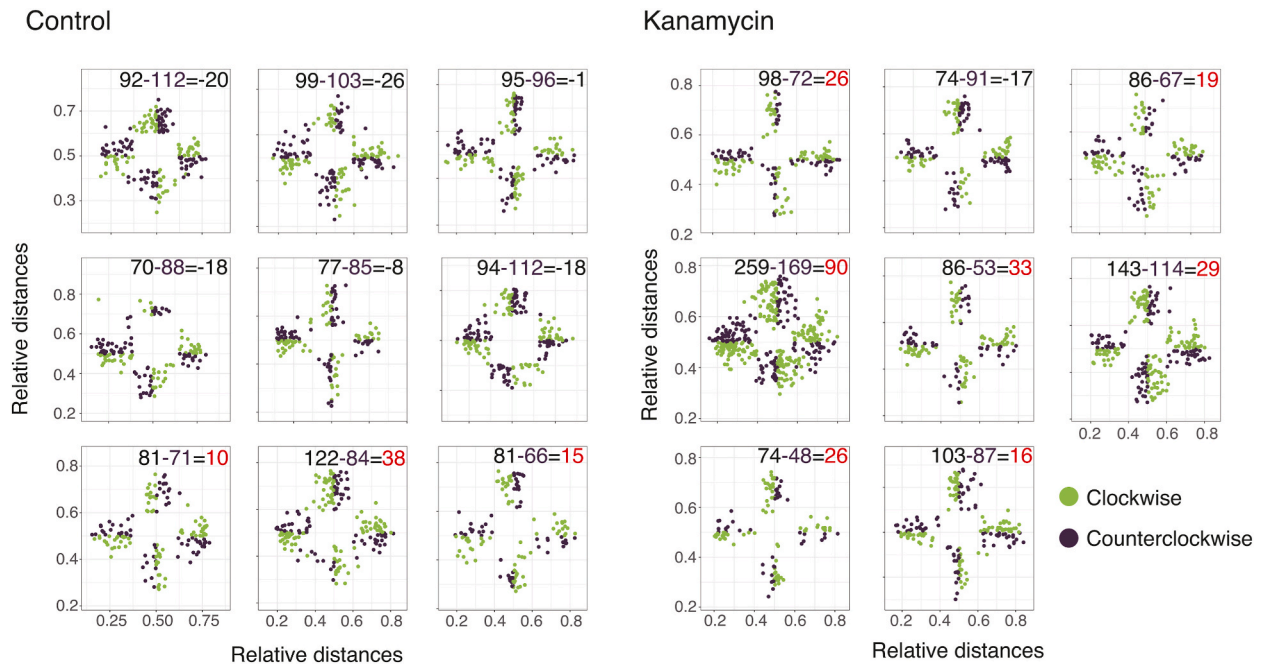
Fig. 8. Clockwise movements in mice with unilateral left inner ear injury. Each plot corresponds to the result from a single mouse in the open field test on day 7. The position of the mouse was recorded as a point where it crossed the middle line close to the cage wall in the next image. Clockwise and counterclockwise movements are colored in green and purple, respectively. To quantify the direction of the movement, a crossing in the clockwise direction was counted as plus one, whereas a crossing in the counterclockwise direction was counted as minus one. The counts are indicated in the upper right corner of each plot. Red numbers indicate positive total counts and a more frequent clockwise crossing of the middle line in the kanamycin group. Each plot corresponds to the result from a single mouse.
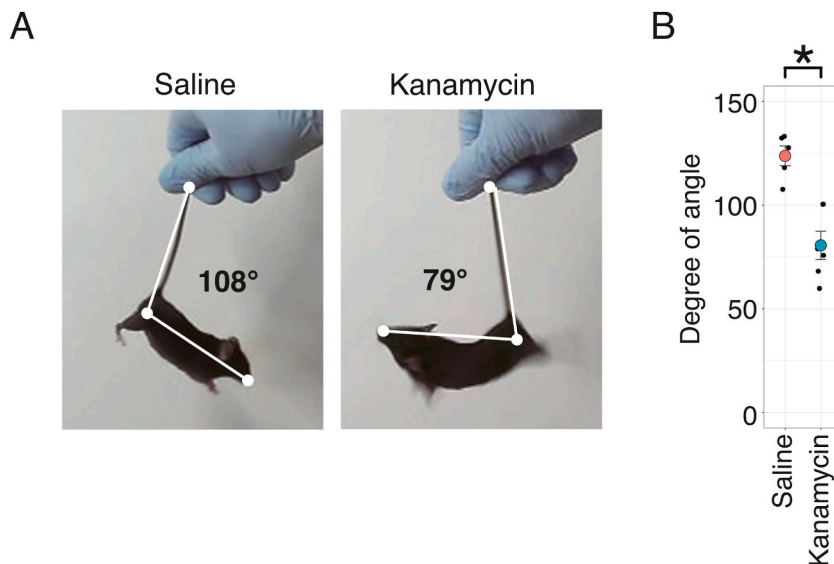

Fig. 9. Tail suspension-rotation test for detecting kanamycin-induced unilateral left inner ear injury. (A) Mice were suspended by their tail, and the tail was twisted to rotate the body. A clockwise rotation induced a strong dorsal bend in the mouse with left unilateral inner ear injury (right panel) compared with the control mouse (left panel). The degree of the angle between the tail and longitudinal body axis was measured from the images of the video recordings. (B) On day 14 postoperatively, the angles in kanamycin-treated mice (red, n = 6) are significantly smaller than those in control mice (green, n = 5). The difference was calculated using the two-sample Wilcoxon test. The error bars show the standard error of the mean. *, p < 0.05.

frequency counts of line crossings, mice with injury in the left ear showed in the open field test more frequently clockwise movements than in the opposite direction. In our mouse model, the tendency of clockwise movement in the kanamycin group lasted for >1 week postoperatively.

4.1. Total distance of movement

The total ambulation distance was increased in the unilateral injury group only on postoperative day 3. In a previous study by Drago et al. on young and old (24-month-old) male Sprague–Dawley rats, surgical unilateral labyrinthectomy reduced movement scores in both age groups [38]. Notably, several experimental conditions differed between their study and our current study. Drago et al. used a surgical procedure by drilling the left inner ear to establish unilateral inner ear injury, whereas we used a round window approach and kanamycin injection. In Drago et al., the movement score increased if both forelegs moved into the next area, whereas our measurement was the actual distance between detected objects in two consecutive images. Moreover, the observation period was 15 min in our study as opposed to the 2 min in the study by Drago et al. In fact, the significant contribution of kanamycin/saline injection was detected by including the entire time course for the analysis (Fig. 6, day 3).

4.2. Frequent movement to the healthy side after unilateral inner ear injury

When mice in the open field test were inspected by a human experimenter on postoperative day 14, sniffing activity in injured mice was less frequent than that in control mice. The deep learning model further found that the time course of the accumulated angle was markedly different between kanamycin-treated and control mice on days 3, 7, and 17 after the injury (Fig. 7). The left inner ear injury resulted in the accumulation of a clockwise turn, toward the healthy side of the right ear, during exploration. Therefore, in our study, mice with unilateral kanamycin injury turned more toward a sound source detected by the healthy ear. The x-y coordinates of mouse positions from three consecutive images were used to calculate the angle of mouse movements, and movements or angles were assumed to have no influence on future movements or angles. Our results from two directions, calculation of the angle and the clockwise movement in the cage, indicated the new finding that unilateral inner ear injury caused more frequent movement toward the healthy side.

4.3. Tail suspension-rotation test

In the tail suspension-rotation test, a physical sign could be induced in mice with unilateral inner ear injury by suspending the mouse by the tail and twisting the tail in a clockwise direction, the direction of the healthy ear, resulting in the fast clockwise rotation of the trunk. During this rotation, dorsal bending of the neck and trunk was observed. In previous studies using rat models with surgical labyrinthectomy or chemical injection of sodium arsanilate into the unilateral tympanic cavity, lifting the rat by the tail induced trunk rotation [39,40]. In one of these studies, the direction of rotation during tail suspension was in good agreement with that of the current study; labyrinthectomy in the right ear induced a counterclockwise rotation during tail suspension [40]. The only difference between this study on mice and previous ones on rats was that in our study, twisting the tail in a clockwise direction was necessary to induce rapid trunk rotation. This rotation sign was sensitive as it was detected in all mice with unilateral inner ear injury on day 14 after the injury but not in any of the mice treated with saline.

4.4. Lasting change for >1 week postoperatively

These results suggested that unilateral inner ear disorders can cause behavioral abnormalities even for >1 week, after the acute phase of injury. Ito et al. reported that unilateral labyrinthectomy with arsanilic acid causes acute vestibular disorder, followed by compensatory mechanisms. They found behavioral abnormalities, such as circling, dystonia, landing, rotation, and head deviation a few days after the surgery, all of which improved by day 7 when vestibular compensation became active [17].

Binaural hearing helps distinguish between multiple sounds based on differences in time, intensity, and frequency spectrum [41, 42]. In unilateral hearing loss, these advantages of binaural hearing are compromised. The significance of these aspects in unilateral hearing loss has been less acknowledged [11]. Unilateral hearing loss in children may influence speech perception and communication, language development, and academic performance and may lead to a potential handicap [43–45]. Therefore, a proper animal model of unilateral hearing loss and its analysis method needs to be developed. Lasting disability and the time course of the compensation in simple behavior are useful for basic research on prevention and treatment.

4.5. Consistency of object detection using the CNN model

Our CNN model located the center of the object detection bounding box without the tail region. This model precisely identified the position and movement of the mouse without a delay in tail movement. In recent reports on deep learning programs, body parts, such as paws, snouts, eyes, and the whole body, are detected as key points, and relative distances between the key points are calculated to extract movement features [23,46]. However, all key points of the body parts are not always detected in images. Beddings in a home cage environment often cover the paws of a mouse. In the recent key point detection work, lost data points were substituted by related data points [23]. Our analysis model managed to place the bounding box of 17 mice over 230,000 images. Therefore, object detection using a bounding box is beneficial for behavior analysis in a relatively complex environment, such as in a home cage with natural

bedding.

Evaluating the object detection results is usually difficult because many images are subjected to the detection. In current practice, models are evaluated based on a limited number of test images with known object locations, in which detection results are compared with the ground truth. We developed a deep learning classification model to score and detect the success and failure of mouse detection using a new set of images. The classification model was evaluated using a ROC curve with a high AUC of 0.98. This classification model was used to confirm all data of >230,000 images. Therefore, the deep learning classification model trained to detect the correct bounding box placement enables us to reliably evaluate the results of object detection.

4.6. Clinical perspective

Detection of unilateral hearing abnormalities from daily behavior in a noninvasive manner is particularly useful in children and older adults because they often cannot accurately describe the hearing problem. Hearing tests for children include other sensory tests, such as ABR and auditory steady-state response tests, which are performed under sedation, and conditioned orientation response audiometry, which observes the behavioral response to a sound [47–50]. In objective testing, accuracy varies greatly depending on the examiner's ability, the circumstances of the examination, and the type of disease. Therefore, training and experience are needed to estimate audiometric thresholds [51]. In addition, the probability of a false-negative ABR screening result is high in newborns [52]. Johnson et al. report that as many as 23 % of cases of neonatal hearing loss might be missed [53]. Therefore, new objective evaluations over time are needed for the early detection of unilateral hearing loss, possibly bridging the gap between preclinical research and clinical application through interdisciplinary collaboration.

The deep learning model found that behavioral changes of unilateral inner ear disorder lasted beyond 1 week in the murine injury model. These lasting behavioral changes are a useful marker for further studies of compensatory processes in injured mice.

Ethical statement

The protocols of all animal experiments were approved by the Animal Care and Use Committee of Jichi Medical University (approval no 24099-01).

Data availability statement

This manuscript has been submitted to bioRxiv (https://doi.org/10.1101/2023.11.04.565603). The datasets analyzed for Figs. 2, 4 and 5 are available from Harvard Dataverse (https://doi.org/10.7910/DVN/VNCTMR) [54]. Code and data for Figs. 6–8 are available from Harvard Dataverse (https://doi.org/10.7910/DVN/RVV1EM).

CRediT authorship contribution statement

Masao Noda: Writing – review & editing, Writing – original draft, Validation, Resources, Project administration, Methodology, Investigation, Formal analysis, Data curation, Conceptualization. **Ryota Koshu:** Project administration, Methodology, Investigation. **Dias Mari Shimada:** Project administration. **Chortip Sajjaviriya:** Project administration, Methodology, Investigation, Data curation. **Chizu Saito:** Project administration. **Makoto Ito:** Project administration, Methodology. **Taka-aki Koshimizu:** Writing – review & editing, Writing – original draft, Visualization, Validation, Supervision, Software, Resources, Project administration, Methodology, Investigation, Funding acquisition, Formal analysis, Data curation, Conceptualization.

Declaration of competing interest

The authors declare that they have no known competing financial interests or personal relationships that could have appeared to influence the work reported in this paper.

Appendix A. Supplementary data

Supplementary data to this article can be found online at https://doi.org/10.1016/j.heliyon.2024.e38938.

References

[1] S. Dhanireddy, W.C. Liles, G.A. Gates, Vestibular toxic effects induced by once-daily aminoglycoside therapy, Arch. Otolaryngol. Head Neck Surg. 131 (2005) 46–48, https://doi.org/10.1001/archotol.131.1.46.

[2] T. Nakashima, M. Teranishi, T. Hibi, M. Kobayashi, M. Umemura, Vestibular and cochlear toxicity of aminoglycosides–a review, Acta Otolaryngol. 120 (2000) 904–911, https://doi.org/10.1080/00016480050218627.

[3] R.E. Ariano, S.A. Zelenitsky, D.A. Kassum, Aminoglycoside-induced vestibular injury: maintaining a sense of balance, Ann. Pharmacother. 42 (2008) 1282–1289, https://doi.org/10.1345/aph.1L001.

[4] D. Konrad-Martin, et al., Applying U.S. national guidelines for ototoxicity monitoring in adult patients: perspectives on patient populations, service gaps, barriers and solutions, Int. J. Audiol. 57 (2018) S3–S18, https://doi.org/10.1080/14992027.2017.1398421.

[5] M. Jiang, T. Karasawa, P.S. Steyger, Aminoglycoside-induced cochleotoxicity: a review, Front. Cell. Neurosci. 11 (2017) 308, https://doi.org/10.3389/fncel.2017.00308.

[6] B. Bowsher, Sensorineural deafness following routine transurethral resection of the prostate, BMJ Case Rep. 2015 (2015), https://doi.org/10.1136/bcr-2015-212933.

[7] A.M. Selleck, K.D. Brown, L.R. Park, Cochlear implantation for unilateral hearing loss, Otolaryngol Clin North Am 54 (2021) 1193–1203, https://doi.org/10.1016/j.otc.2021.07.002.

[8] P. Mick, I. Kawachi, F.R. Lin, The association between hearing loss and social isolation in older adults, Otolaryngol. Head Neck Surg. 150 (2014) 378–384, https://doi.org/10.1177/0194599813518021.

[9] L.L. Cunningham, D.L. Tucci, Hearing loss in adults, N. Engl. J. Med. 377 (2017) 2465–2473, https://doi.org/10.1056/NEJMra1616601.

[10] D.P. Kumpik, A.J. King, A review of the effects of unilateral hearing loss on spatial hearing, Hear. Res. 372 (2019) 17–28, https://doi.org/10.1016/j.heares.2018.08.003.

[11] H.A. Snapp, S.A. Ausili, Hearing with one ear: consequences and treatments for profound unilateral hearing loss, J. Clin. Med. 9 (2020), https://doi.org/10.3390/jcm9041010.

[12] R.C. Nelissen, M.J. Agterberg, M.K. Hol, A.F. Snik, Three-year experience with the Sophono in children with congenital conductive unilateral hearing loss: tolerability, audiometry, and sound localization compared to a bone-anchored hearing aid, Eur. Arch. Oto-Rhino-Laryngol. 273 (2016) 3149–3156, https://doi.org/10.1007/s00405-016-3908-6.

[13] P. Van de Heyning, et al., Incapacitating unilateral tinnitus in single-sided deafness treated by cochlear implantation, Ann. Otol. Rhinol. Laryngol. 117 (2008) 645–652, https://doi.org/10.1177/000348940811700903.

[14] M.A. Blasco, M.I. Redleaf, Cochlear implantation in unilateral sudden deafness improves tinnitus and speech comprehension: meta-analysis and systematic review, Otol. Neurotol. 35 (2014) 1426–1432, https://doi.org/10.1097/MAO.0000000000000431.

[15] A. Buechner, et al., Cochlear implantation in unilateral deaf subjects associated with ipsilateral tinnitus, Otol. Neurotol. 31 (2010) 1381–1385, https://doi.org/10.1097/MAO.0b013e3181e3d353.

[16] J.P. Thomas, K. Neumann, S. Dazert, C. Voelter, Cochlear implantation in children with congenital single-sided deafness, Otol. Neurotol. 38 (2017) 496–503, https://doi.org/10.1097/MAO.0000000000001343.

[17] T. Ito, et al., Vestibular compensation after vestibular dysfunction induced by arsanilic acid in mice, Brain Sci. 9 (2019), https://doi.org/10.3390/brainsci9110329.

[18] R. Wijesinghe, A. Camp, The intrinsic plasticity of medial vestibular nucleus neurons during vestibular compensation-a systematic review and meta-analysis, Syst. Rev. 9 (2020) 145, https://doi.org/10.1186/s13643-020-01399-2.

[19] K.F. Hamann, J. Lannou, Dynamic characteristics of vestibular nuclear neurons responses to vestibular and optokinetic stimulation during vestibular compensation in the rat, Acta Otolaryngol Suppl 445 (1987) 1–19, https://doi.org/10.3109/00016488809099006.

[20] M.N. McDonnell, S.L. Hillier, Vestibular rehabilitation for unilateral peripheral vestibular dysfunction, Cochrane Database Syst. Rev. 1 (2015) CD005397, https://doi.org/10.1002/14651858.CD005397.pub4.

[21] R.A. Dobie, F.O. Black, S.C. Pezsnecker, V.L. Stallings, Hearing loss in patients with vestibulotoxic reactions to gentamicin therapy, Arch. Otolaryngol. Head Neck Surg. 132 (2006) 253–257, https://doi.org/10.1001/archotol.132.3.253.

[22] T.D. Pereira, et al., SLEAP: a deep learning system for multi-animal pose tracking, Nat. Methods 19 (2022) 486–495, https://doi.org/10.1038/s41592-022-01426-1.

[23] M. Bogachev, et al., Video-based marker-free tracking and multi-scale analysis of mouse locomotor activity and behavioral aspects in an open field arena: a perspective approach to the quantification of complex gait disturbances associated with Alzheimer's disease, Front Neuroinform 17 (2023) 1101112, https://doi.org/10.3389/fninf.2023.1101112.

[24] D. Buhler, et al., Leptin deficiency-caused behavioral change - a comparative analysis using EthoVision and DeepLabCut, Front. Neurosci. 17 (2023) 1052079, https://doi.org/10.3389/fnins.2023.1052079.

[25] O. Sturman, et al., Deep learning-based behavioral analysis reaches human accuracy and is capable of outperforming commercial solutions, Neuropsychopharmacology 45 (2020) 1942–1952, https://doi.org/10.1038/s41386-020-0776-y.

[26] K. Kawakami, et al., Evaluation of bedding and nesting materials for laboratory mice by preference tests, Exp. Anim. 56 (2007) 363–368, https://doi.org/10.1538/expanim.56.363.

[27] J. Freymann, P.P. Tsai, H. Stelzer, H. Hackbarth, The amount of cage bedding preferred by female BALB/c and C57BL/6 mice, Lab Anim (NY) 44 (2015) 17–22, https://doi.org/10.1038/laban.659.

[28] J. Freymann, P.P. Tsai, H.D. Stelzer, R. Mischke, H. Hackbarth, Impact of bedding volume on physiological and behavioural parameters in laboratory mice, Lab Anim 51 (2017) 601–612, https://doi.org/10.1177/0023677217694400.

[29] A.N. Heeringa, R.A. Stefanescu, Y. Raphael, S.E. Shore, Altered vesicular glutamate transporter distributions in the mouse cochlear nucleus following cochlear insult, Neuroscience 315 (2016) 114–124, https://doi.org/10.1016/j.neuroscience.2015.12.009.

[30] C. Zeng, N. Nannapaneni, J. Zhou, L.F. Hughes, S. Shore, Cochlear damage changes the distribution of vesicular glutamate transporters associated with auditory and nonauditory inputs to the cochlear nucleus, J. Neurosci. 29 (2009) 4210–4217, https://doi.org/10.1523/JNEUROSCI.0208-09.2009.

[31] M.D. Shimada, et al., Macrophage depletion attenuates degeneration of spiral ganglion neurons in kanamycin-induced unilateral hearing loss model, Sci. Rep. 13 (2023) 16741, https://doi.org/10.1038/s41598-023-43927-9.

[32] W. Liu, et al., SSD: single shot MultiBox detector, arXiv e-prints (2015) 02325 arXiv:1512.

[33] T.-Y. Lin, et al., Microsoft COCO: common objects in context, arXiv e-prints, arXiv:1405.0312 (2014). https://ui.adsabs.harvard.edu/abs/2014arXiv1405.0312L.

[34] J. Huang, et al., Speed/accuracy trade-offs for modern convolutional object detectors, arXiv e-prints, arXiv:1611.10012 (2016). https://ui.adsabs.harvard.edu/abs/2016arXiv161110012H.

[35] W. Hadley, ggplot2: Elegant Graphics for Data Analysis, Springer-Verlag, New York, 2016.

[36] R.C.R. Team, A language and environment for statistical computing. https://www.R-project.org/, 2011.

[37] F. Chollet, Xception: deep learning with depthwise separable convolutions, in: 2017 IEEE Conference on Computer Vision and Pattern Recognition (CVPR), 2016, pp. 1800–1807.

[38] F. Drago, L. Nardo, L. Rampello, R. Raffaele, Vestibular compensation in aged rats with unilateral labyrinthectomy treated with dopaminergic drugs, Pharmacol. Res. 33 (1996) 135–140, https://doi.org/10.1006/phrs.1996.0020.

[39] M.A. Hunt, S.W. Miller, H.C. Nielson, K.M. Horn, Intratympanic injection of sodium arsanilate (atoxyl) solution results in postural changes consistent with changes described for labyrinthectomized rats, Behav. Neurosci. 101 (1987) 427–428, https://doi.org/10.1037//0735-7044.101.3.427.

[40] M. Hitier, S. Besnard, G. Vignaux, P. Denise, S. Moreau, The ventrolateral surgical approach to labyrinthectomy in rats: anatomical description and clinical consequences, Surg. Radiol. Anat. 32 (2010) 835–842, https://doi.org/10.1007/s00276-010-0690-9.

[41] J. Muller, F. Schon, J. Helms, Speech understanding in quiet and noise in bilateral users of the MED-EL COMBI 40/40+ cochlear implant system, Ear Hear. 23 (2002) 198–206, https://doi.org/10.1097/00003446-200206000-00004.

[42] P. Schleich, P. Nopp, P. D'Haese, Head shadow, squelch, and summation effects in bilateral users of the MED-EL COMBI 40/40+ cochlear implant, Ear Hear. 25 (2004) 197–204, https://doi.org/10.1097/01.aud.0000130792.43315.97.

[43] H. Steven Colburn, B. Shinn-Cunningham, G. Kidd Jr., N. Durlach, The perceptual consequences of binaural hearing, Int. J. Audiol. 45 (Suppl 1) (2006) S34–S44, https://doi.org/10.1080/14992020600782642.

[44] M.N. Ruscetta, E.M. Arjmand, S.R. Pratt, Speech recognition abilities in noise for children with severe-to-profound unilateral hearing impairment, Int. J. Pediatr. Otorhinolaryngol. 69 (2005) 771–779, https://doi.org/10.1016/j.ijporl.2005.01.010.

[45] H. Noh, Y.G. Park, How close should a student with unilateral hearing loss stay to a teacher in a noisy classroom? Int. J. Audiol. 51 (2012) 426–432, https://doi.org/10.3109/14992027.2012.654855.

[46] A. Mathis, et al., DeepLabCut: markerless pose estimation of user-defined body parts with deep learning, Nat. Neurosci. 21 (2018) 1281–1289, https://doi.org/10.1038/s41593-018-0209-y.

[47] S.E. Nielsen, S.O. Olsen, Validation of play-conditioned audiometry in a clinical setting, Scand. Audiol. 26 (1997) 187–191, https://doi.org/10.3109/01050399709074992.

[48] S. Hatzopoulos, et al., Estimation of pure-tone thresholds in adults using extrapolated distortion product otoacoustic emission input/output-functions and auditory steady state responses, Int. J. Audiol. 48 (2009) 625–631, https://doi.org/10.1080/14992020902998391.

[49] M. Tanaka, et al., Discrepancy between auditory brainstem responses, auditory steady-state responses, and auditory behavior in two patients with Pelizaeus-Merzbacher disease, Auris Nasus Larynx 35 (2008) 404–407, https://doi.org/10.1016/j.anl.2007.09.002.

[50] A. Ciorba, et al., Identifying congenital hearing impairment: preliminary results from a comparative study using objective and subjective audiometric protocols, Acta Otorhinolaryngol. Ital. 33 (2013) 29–35.

[51] J. Gravel, et al., New York State universal newborn hearing screening demonstration project: effects of screening protocol on inpatient outcome measures, Ear Hear. 21 (2000) 131–140, https://doi.org/10.1097/00003446-200004000-00007.

[52] Y. Levit, M. Himmelfarb, S. Dollberg, Sensitivity of the automated auditory brainstem response in neonatal hearing screening, Pediatrics 136 (2015) e641–e647, https://doi.org/10.1542/peds.2014-3784.

[53] J.L. Johnson, et al., A multicenter evaluation of how many infants with permanent hearing loss pass a two-stage otoacoustic emissions/automated auditory brainstem response newborn hearing screening protocol, Pediatrics 116 (2005) 663–672, https://doi.org/10.1542/peds.2004-1688.

[54] G. King, An introduction to the Dataverse network as an infrastructure for data sharing, Socio. Methods Res. 36 (2007) 173–199.